

Return from Dormancy: Rapid inflation and seismic unrest at Mt. Edgecumbe (L'úx Shaa) Volcano, Alaska

Ronni Grapenthin^{1,2}, Yitian Cheng^{1,2}, Mario Angarita^{1,2}, Darren Tan^{1,2}, Franz J. Meyer^{1,3}, David Fee^{1,2}

¹Geophysical Institute & Dept. of Geoscience, University of Alaska Fairbanks

²Alaska Volcano Observatory, Geophysical Institute, University of Alaska Fairbanks

³Alaska Satellite Facility, University of Alaska Fairbanks

Key Points:

- InSAR time series reveal up to 8.7 cm/yr of inflation at Mt. Edgecumbe in satellite line-of-sight
- Constant inflation begins in August 2018, microseismicity in July 2019, larger earthquakes in 2020
- Bayesian modeling suggests magma recharge into a 14 deg westward dipping sill ranging from 5.3-7.6 km depth

Corresponding author: Ronni Grapenthin, rgrapenthin@alaska.edu

Abstract

In April 2022 a seismic swarm near Mt. Edgecumbe in southeast Alaska suggests renewed activity at this dormant volcano located in a transform fault setting. Oral Tlingit history describes low-level basaltic eruptions ≈ 800 years ago. Thin rhyolitic tephra deposited 5–4 ka. We analyze synthetic aperture radar data from 2014–2022 and resolve rapid inflation up to 8.7 cm/yr beginning in August 2018. Bayesian modeling suggests a gently westward dipping sill opened 0.65 m between 7.6 km to 5.3 km depth, centered about 2–3 km east of Mt. Edgecumbe. Reanalyzed seismicity, recorded 25 km away, shows increased activity since July 2019. We hypothesize mafic magma ascent through ductile material, accumulating below a silicic seal or in a silicic reservoir, and triggering seismicity in the overburden. Cloud-native open data and workflows enabled discovery and analysis of this rapid inflation within days after going unnoticed for >3 years.

Plain Language Summary

In April 2022 a cluster of earthquakes detected near Mt. Edgecumbe in Southeast Alaska suggested magmatic activity. As the volcano is near the major Queen-Charlotte Fairweather fault that separates the Pacific and North American plates, similar earthquakes were previously assumed to be tectonic in nature. Since magmatic activity at volcanoes is often accompanied by ground deformation, we analyzed available satellite radar data going back to fall of 2014. This reveals crustal motion toward the satellite of up to 8.7 cm/yr starting in August 2018, which totalled up to 27 cm by November 2021. Modeling of the deformation suggests that magma is intruding between 5–8 km depth into a gently dipping tabular body. Since the nearest seismograph is 25 km away, we record only large seismicity, which increases in July 2019, but we perhaps missed some lower energy seismicity due to this distance. We believe that we are observing magma rising through somewhat malleable crust into an existing magmatic system and that the observed earthquakes are created as the overlying rock adjusts to the increased magmatic pressure. The observed activity is rare, especially in similar tectonic settings, and presents an opportunity to better understand the reactivation of dormant volcanoes.

1 Introduction

Located in Southeast Alaska, the home to about 73,000 people, or 10% of the state's population, Mount Edgecumbe (L'ux Shaa in Tlingit) is part of the Mt. Edgecumbe Volcanic Field on Kruzof Island on the west side of Sitka Sound (Figure 1). The eastern shore of Sitka Sound, about 25 km away from Mount Edgecumbe, is home to the almost 8,500 residents of Sitka, and destination of projected 200,000–400,000 cruise passengers in 2022 (Woolsey, 2021). Like most communities in Southeast Alaska, including the state capital Juneau, Sitka is only accessible via air and sea, as no connections to the highway system exist, and thus quite vulnerable to hazards due to earthquakes, tsunamis and volcanic eruptions, especially volcanic ash.

On April 11, 2022, a Sitka resident noted that the openly available Alaska Earthquake Center's (AEC) location for an M2.1 earthquake was under Mt. Edgecumbe and inquired with Alaska Volcano Observatory (AVO) contacts whether this earthquake is related to the volcano or, as previously suggested for seismicity in the region, purely tectonic. As this dormant volcano is not monitored with a dedicated geophysical instrument network, the review of seismicity relies on the broadly distributed regional seismic network, and the related location uncertainties. Activity recorded by the closest seismograph SIT, 25 km away in Sitka, indicated that a seismic swarm started about 02:00 am AKDT on April 11, 2022. Earthquakes located by the AEC range in magnitude from 1.0–2.7 and appear broadly distributed to the NE of Mt. Edgecumbe near the eastern rim of Crater Ridge (Figure 1, red circles in inset). This swarm, with estimated depths ranging from about 1–12 km, was preceded by a burst of located seismic activity in 2020 that began

with an M3.0 earthquake on 2020-01-02 and lasted until about mid-2021. With the caveat of kilometer-scale uncertainties in the published locations, the depth ranges of both swarms appear similar, but epicenter locations seem more tightly clustered and slightly shifted southward in 2022 than before (compare blue and red circles in Figure 1, inset). No other seismicity in this region has been large enough to allow for location estimation through the regional network before 2020 while seismicity of similar magnitudes has been consistently recorded offshore (Figure 1).

To investigate the origin of these earthquakes and their relation to the volcano, we use Sentinel-1 (Torres et al., 2012) synthetic aperture radar (SAR) observations to perform cloud-based interferometric SAR (InSAR) time series analysis on Mt. Edgecumbe. Using seasonal data that omits winter acquisitions from 2014-10-17 until 2021-11-27, we find rapid inflation that began abruptly in August 2018. Ground motion in the line of sight of the satellite reaches velocities of 8.7 cm/yr. We perform a Bayesian inversion of the InSAR velocity field, which suggests magma accumulation in a dipping body at about 5-7 km depth beneath the volcano. Our reanalysis of microseismicity on the closest seismograph in Sitka indicates an uptick in recorded seismicity beginning in July 2019.

2 Background

Perhaps popularly best known for a very elaborate 1974 April Fools joke, when the local Oliver “Porky” Bickar set 70 old tires on fire in Mt. Edgecumbe’s crater, making Sitka’s residents believe that the volcano was erupting, the Mt. Edgecumbe volcanic field has a rich history of volcanism, including felsic lavas and pyroclastic flows. Vents are linearly organized, trending northeast from the southwestern tip of Kruzof Island to Mud Bay in the northeast, perhaps aligned with a crustal fissure (Riehle et al., 1992). The most recent report of activity is part of Tlingit oral history and reports “a mountain blinking, spouting fire and smoke” 800-900 years ago (Kitka, n.d.). During the Holocene, for 5.8 and 4.2 ka, Riehle et al. (1992) report two eruptions that created thin rhyolite layers on Kruzof Island, which they attribute to Crater Ridge. Prior to that, from about 14.6-13.1 ka Praetorius et al. (2016) document increased volcanism with a recurrence of about 1.5 events per century that they attribute to last glacial maximum ice loss as reported for, e.g., Iceland (e.g., Jull & McKenzie, 1996; MacLennan et al., 2002; Pagli & Sigmundsson, 2008) and California (Jellinek et al., 2004). This activity ranged from basaltic to late erupting rhyolite, the latter also found in adjacent marine sediment cores in tephra-fall and pyroclastic flow deposits (Addison et al., 2010). Based on the eruptive sequence of basalt and andesite throughout the existence of the field and late erupting rhyolite, Riehle et al. (1992) suggest basaltic underplating created the system and produced a stratified magma chamber with a low density high viscosity rhyolite cap.

In addition to volcanic activity and deformation induced by Last Glacial Maximum deglaciation, this region also experiences more recent Glacial Isostatic Adjustment (GIA). Larsen et al. (2005) attribute the rapid uplift since the late 1700s to viscoelastic relaxation of the mantle following the retreat of Little Ice Age glaciers. Ongoing glacial retreat continues to induce an elastic and viscoelastic response of the Earth measured by GPS (Larsen et al., 2004; J. L. Elliott et al., 2010). Hu and Freymueller (2019) link ongoing variations in this uplift to accelerations in ice mass loss between the 1990s and 2012, as documented elsewhere (Compton et al., 2015).

Tectonically, the Edgecumbe volcanic field is located near the Fairweather-Queen Charlotte transform fault (45-46 mm/yr slip rate) to the west, accommodating most of the Pacific-North America relative plate motions (J. Elliott & Freymueller, 2020a). As such, this fault system experiences frequent large strike slip earthquakes, such as the 1972 M7.6 Sitka earthquake just south of Kruzof Island (Schell & Ruff, 1989). This region is located on the slightly northward translating (about 3 mm/yr) Baranof block (J. Elliott & Freymueller, 2020a). While this region has generally been understood to also exhibit

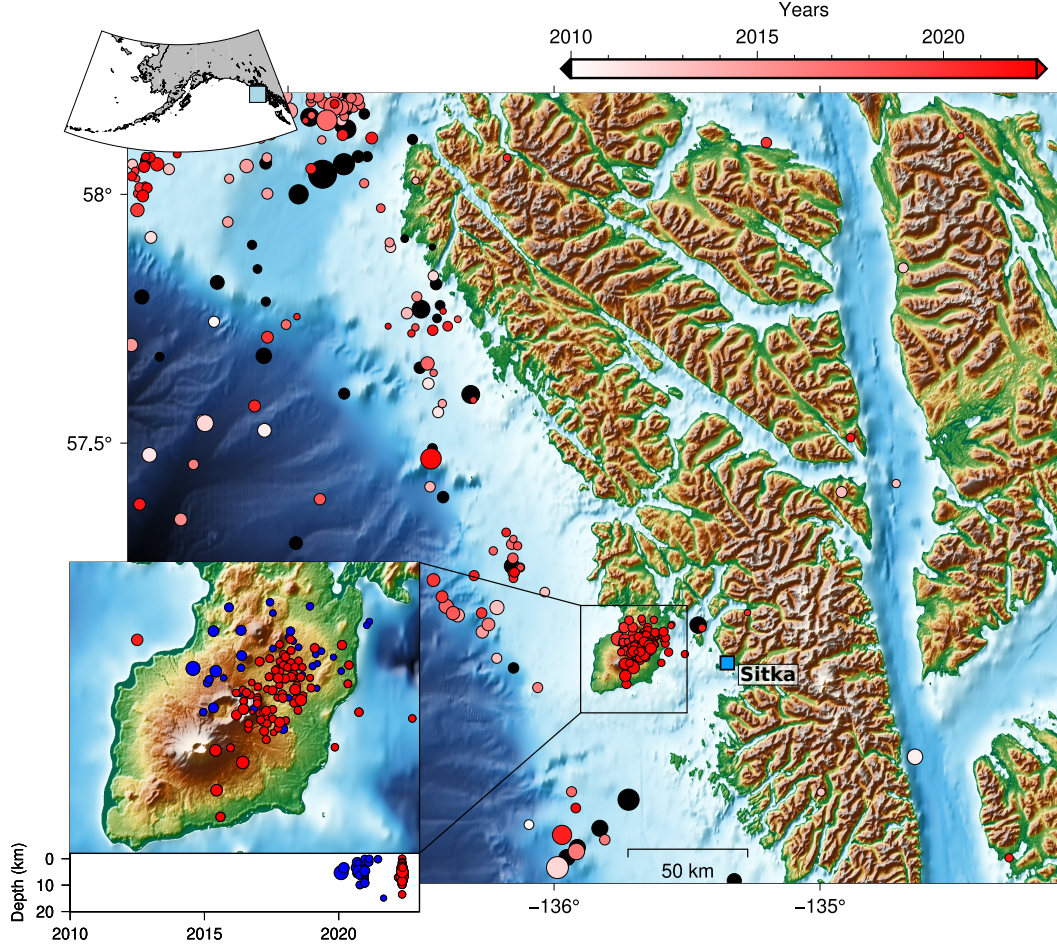


Figure 1. Mt. Edgecumbe overview map. Main map shows topography and regional seismicity from 1990-01-01 until 2022-04-18 (earthquake locations from Alaska Earthquake Center retrieved via USGS ANSS catalog). Earthquakes before 2010 are colored black, from 2010 onward according to colorbar. Blue square shows location of town of Sitka. Bottom inset shows close up of Kruzof Island seismicity mainly NE of Mt. Edgecumbe with a time-depth plot illustrating the absence of earthquakes in that region before 2020, blue earthquakes occurred before 2022, red earthquakes in 2022. Top inset shows location of main map in SE Alaska.

small rates of fault normal convergence (e.g., J. Elliott & Freymueller, 2020a), more recent data and modeling allow for small amounts of extension in this area (J. Elliott & Freymueller, 2020b), perhaps supporting the volcanism here.

3 Data & Methods

We use synthetic aperture radar data acquired between 2014-10-17 and 2021-11-27 by the European Space Agency’s Sentinel-1 mission (Torres et al., 2012) on ascending path 174 and frame 402. Recently, Sentinel-1B was tasked with the observation of this scene, but it remains unobserved since December 2021 due to an anomaly in the satellite’s power system (ESA, 2022). Other scenes do not capture the full island, but more importantly, they do not reach back in time until 2014. Hence, we utilize this observation geometry in this project.

We use the on-demand InSAR capabilities embedded in NASA Alaska Satellite Facility’s (ASF) Hybrid Pluggable Processing Pipeline (HyP3) (Hogenson et al., 2016; Johnston et al., 2022) that employs GAMMA (Wegmüller et al., 2016) to process 126 SAR scenes into 405 interferograms with a temporal baseline of 48 days within one season. We assume decorrelation due to winter weather to be large and hence omit data between December 1 and March 1. We bridge each winter season with at least 3 InSAR pairs. The first image in this stack, acquired on 2014-10-17, serves as the reference image that all remaining repeat acquisitions are aligned to. We use a MintPy (Yunjun et al., 2019) workflow run within ASF’s cloud-based OpenSARLab platform (Hogenson et al., 2021; Meyer et al., 2021) to perform SBAS-based (Berardino et al., 2002) time series analysis of the interferogram stack. Our workflow rejects interferograms below 0.7 temporal and 0.7 spatial average coherence, and performs atmospheric correction using the ERA-5 atmospheric models (Hersbach et al., 2020). Residual topographic errors were estimated and corrected using the approach by Fattahi and Amelung (2013), and phase unwrapping error correction was performed using a phase bridging method in which coherent components with the smallest distance from each other are assumed connected and a smooth phase variation across them is enforced (Chen & Zebker, 2002).

To isolate and model volcanic signals, we reference the resulting InSAR phase time series to a location on Kruzof Island, but away from the volcanic deformation (Figure 2). We then downsample the cumulative LOS displacements using a variance-based algorithm (Agram & Jolivet, 2012) to appropriately weight near and far field pixels according to the information they carry. The downsampled displacement field with 3613 pixels (Figure 4) is then used as input to a Markov-Chain Monte-Carlo (MCMC) based Bayesian inversion approach that utilizes Metropolis-Hastings sampling (e.g., Haario et al., 2001; Aster et al., 2019) implemented in the pymc (Patil et al., 2010) library. We assume a uniform prior distribution of the input parameter space and generate 1 million sample solutions after a 10^5 sample burn-in period. To reduce autocorrelation, we only use every 10^4 sample to estimate the posterior distribution. We test several analytical solutions that relate subsurface pressure changes to surface deformation including a pressure point source (Mogi, 1958), a more general spheroid (Yang et al., 1988), and circular (Fialko et al., 2001) and rectangular (Okada, 1992) sill-like sources. For the circular sill model (Fialko et al., 2001) we generated only 10^5 sample solutions following a 10^4 sample burn-in period using only every 10^2 sample to estimate the solution due to the computational cost of calculating each solution. The overall preferred geometry is determined based on misfit minimization between observations and the most-likely solution, as well as statistical methods (F-test, e.g., Press et al. (2007)) to ensure the fit to the data for any given model improves appropriately with the additional degrees of freedom introduced with each model.

In order to investigate the possibility of contemporaneous seismic unrest not captured in existing seismic catalogs, we implement the REDPy detection algorithm (Hotovec-

Ellis & Jeffries, 2016) to analyze data recorded at the closest seismic station SIT. REDPy utilizes a standard short-time average/long-time average (STA/LTA) algorithm (Allen, 1978) to trigger on events, before cross-correlating events with successive triggers in an attempt to group them into families. REDPy has been used to quantify the temporal evolution of repeating seismicity at several other volcanic settings (e.g., Hotovec-Ellis et al., 2022; Wellik et al., 2021). To focus on swarm-like clusters of events, we opt for a relaxed STA/LTA trigger ratio of 4 on data filtered between 1 and 10 Hz, and a high cross-correlation threshold of 0.7 to group up events. We also manually inspect each cluster and remove all clusters that are dominated by false detections (details in Text S1).

4 Results

The InSAR time series analysis (sample wrapped phase observations in Figures S1-S4; all re-wrapped phase observations in Figure S5) resolves a circular feature of motion toward the satellite (uplift and horizontal motion toward the satellite), perhaps slightly elongated along the NS axis, with a diameter of approximately 17 km (Figure 2). In the satellite line-of-sight, the deformation appears centered about 2-3 km to the east of Mt. Edgumbe (Figure 2a). The LOS shortening reaches a maximum cumulative displacement of about 27 cm, tapering off roughly symmetrically toward the edges of the deformation signal. Figures 2(1-4) show time series of 4 representative pixels marked in Figure 2a. Except for possible seasonal deformation, likely driven by seasonal hydrologic or cryospheric effects (e.g., Heki, 2001; Grapenthin et al., 2006; Borsa et al., 2014), the time series show no substantial deformation from October 2014 until August 2018. At that time, effectively linear deformation began at rates of up to 8.7 cm/yr in the satellite line-of-sight. Supplementary Figure S6 shows the time series of displacement accumulation in map view for all 126 time steps.

The seismicity panel of Figure 2 presents the results of the seismic reanalysis from 2018 until November 2021, the time span covered by the InSAR analysis; data until April 2022 are included in Figure S7. The monthly event detections (gray bars) do not notably increase above background rates until July 2019. They taper off by the beginning of 2020 only to increase again in the middle of 2020 from which point on seismic activity appears elevated until the end of 2021, as reflected in the gradient of the cumulative seismicity. The most recent swarm in April 2022 leads to the most detections compared to any prior time (Figure S7).

We model high coherence (> 0.3) components of the variance-based downsampled InSAR velocities from August 2018 until November 2021 with classic analytical solutions for subsurface volume changes. Figure 3 shows the results of the MCMC inversion in the form of posterior probability density functions (PDF) for each parameter of both sill models along the respective diagonal (point source and spheroid results are in Figures S8-9). The off-diagonal panels show the combined PDFs of parameter pairs where circular pattern indicate largely independent parameters and deviations from circular to elliptical or linear highlight trade-offs between parameters. We find some trade-offs between rectangular sill width, length, opening and depth where, for instance, greater depth would allow for slightly larger opening, and smaller area of the sill would require slightly larger opening. Overall, the ranges of these trade-offs are small (100s of meters for spatial parameters, about 1 cm for opening). Distances of the horizontal location of the source (x , y) are given with respect to the center of the displacement field at 57.0843 deg N and 135.7196 deg W, a location on Crater Ridge (see Figure 4).

We use the most likely values for each parameter of each model to predict the surface deformation in the satellite LOS and show the results for the sill models in Figure 4 (point source and spheroid results are in Figures S8-S9). The top two rows of this figure show the variance-based downsampled deformation results, upon which the parameter estimation and model selection is based, and the bottom two rows show full reso-

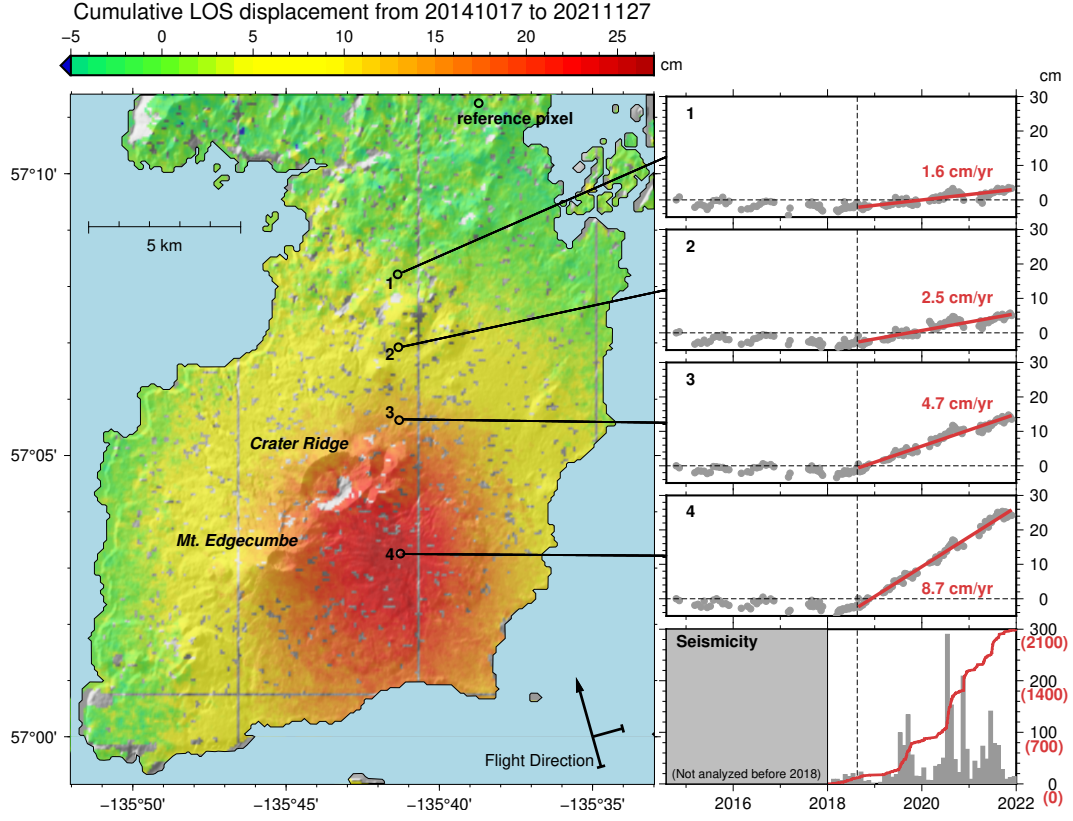


Figure 2. Cumulative line-of-sight displacement map inferred from path 174, frame 402 Sentinel-1A/B SAR data between 2014-10-17 and 2021-11-27. Regional deformation due to tectonics and GIA is largely removed by referencing the local deformation to the observations at the marked reference pixel. Points 1-4 indicate the locations for the time series to the right, showing no or only subtle seasonal deformation until August 2018 followed by a sharp inflection with annual deformation rates of up to 8.7 cm/yr. Right bottom panel shows monthly earthquake counts (gray) and cumulative seismicity (red) from Jan 2018-Dec 2021 on station AT.SIT inferred using a trigger and clustering technique (REDPy). Note that this time period does not include the April 2022 swarm as Sentinel 1B has not been acquiring data since December 2021. Figure S7 includes the most recent seismic data.

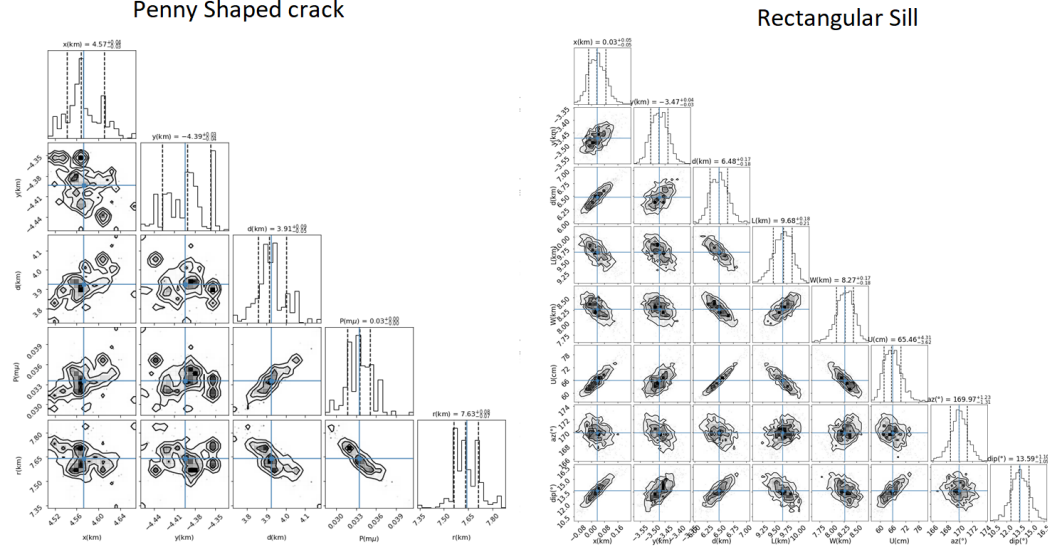


Figure 3.

lution results. Both the penny-shaped crack (Figure 4, middle column) and the rectangular sill (Figure 4, right column) visually reproduce the observations. Both models show slight residuals around Mt. Edgumbe, slightly more prominent in the circular sill model.

To formally evaluate the goodness-of-fit of the most likely parameters we calculate the reduced χ^2_ν statistic, which is slightly lower for the rectangular sill model (33.2 cm) than for the circular sill (37.2 cm). Point source and spheroid have much higher χ^2_ν values (59.6 cm and 82.3 cm, respectively), thus we reject those models. An F-test (Tables S1-S2) confirms that the 3 additional parameters of a the rectangular sill model are justified based on the improvement in fit to the data. Hence, our preferred model is a rectangular sill with most likely parameters values that its center about 3.5 km to the south of Crater Ridge and East of Mt. Edgumbe, dipping about 14 degrees to the West and striking about 11 degrees east of south. With its center at about 6.5 km depth, 9.7 km length and 8.3 km width the top and bottom edges of the sill at about 5.3 km and 7.6 km depth, respectively. The total opening from August 2018 until November 2018 is about 65 cm. Assuming incompressible magma, this yields a total volume change of about $52.33 \times 10^6 \text{ m}^3$.

5 Discussion

Given the large volume of highly coherent SAR data, about 4 years of effectively zero or “background” deformation, clear signals in the sample year-to-year wrapped interferograms, and the sharp change in deformation across the region at the same time, we have high confidence that the InSAR data reveal a physical signal related to localized ground deformation from volcanic activity. The lack of correlation between the signal and the existing and relatively low topography over the island further suggests a physical process. Topographic error correction using the approach by Fattahi and Amelung (2013) showed no significant indications of topographic error in the phase observations. We find that phase referencing to our reference pixel effectively removes tectonic and GIA related contributions. Given the large spatial wavelengths of these signals, we expect any residual motion across the observed area to be very small and non-consequential given the large magnitude of the observed signal. Further, our seismic analysis reveals a grad-

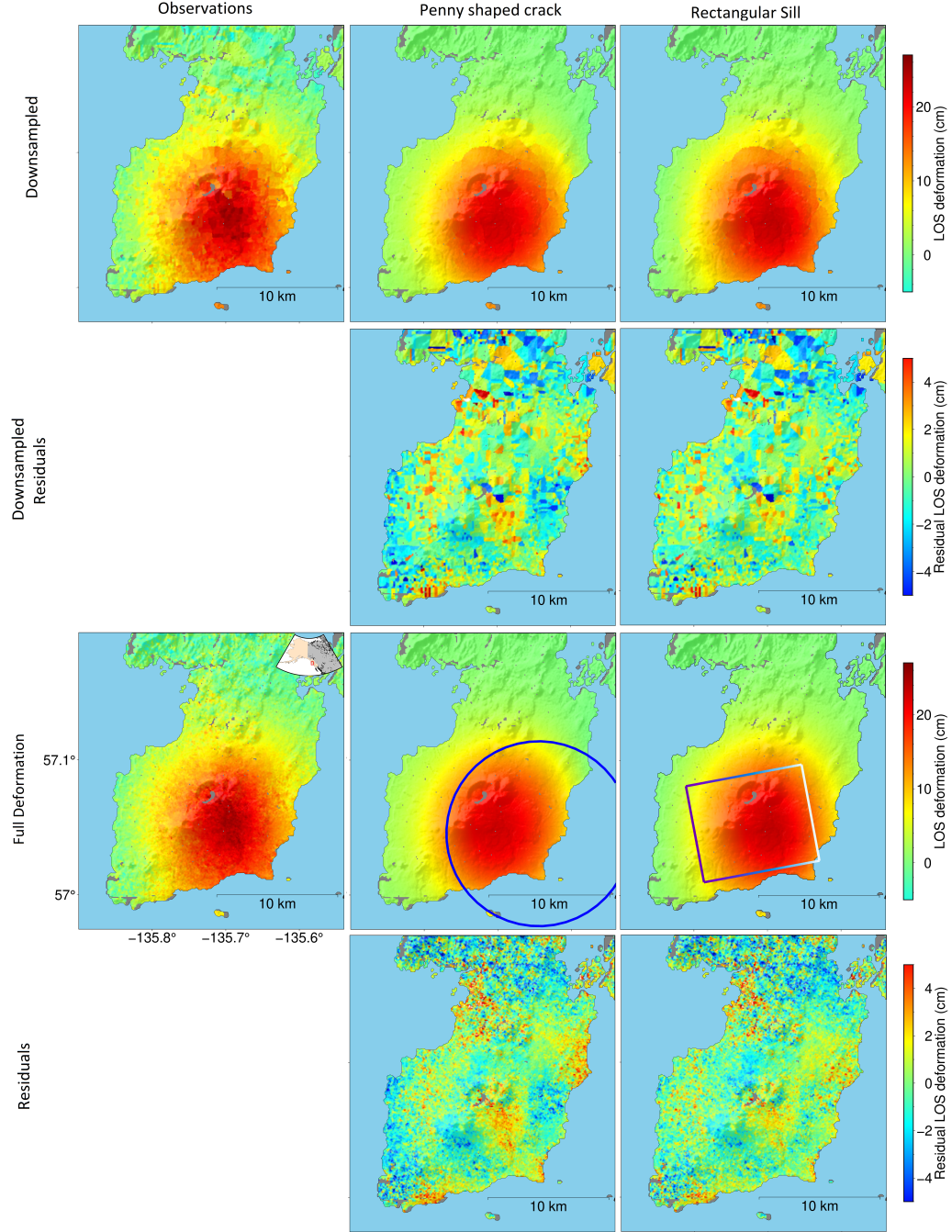


Figure 4.

Observations (left column), penny-shaped crack model predictions and data residuals (middle column), and rectangular sill model predictions and data residuals (right column). Top two rows are at variance-based down-sampled resolution, bottom two rows are at observation resolution. Model estimation and F-test are done for down-sampled residuals.

ual increase in seismicity above background starting from July 2019. Comparisons with earthquakes located by AEC and retrieved via the USGS ANSS catalog show coincident spikes in seismicity from 2020 onward as well, providing added credibility to our seismic analysis (Figure S7).

Modeling the deformation with a slightly dipping sill fits the observations well. Statistical analysis of data residuals prefers this model over other geometries. Slight residuals in the center of the deformation signal may be due to planar geometry assumptions or, perhaps, smaller deformation sources projecting away from the sill. The comparison between the residuals of horizontal circular sill and the dipping rectangular sill shows that the misfit in this region is substantially reduced by the dip (as other tests with horizontal rectangular sills also showed).

Due to the long dormancy of the system we expect that the crust surrounding any remnant magma body is relatively cool and thus viscous effects seem unlikely over the observed time spans. This is also reflected in the InSAR time series, which show largely linear motion (with superimposed small amplitude seasonal effects) after August 2018, suggesting that the source geometry is stable over time and volume change rates are fairly constant.

Based on lacking basalt inclusions in Edgumbe rhyolites and pyroclasts, Riehle et al. (1992) suggest a compositionally stratified magma chamber capped by a highly viscous, low density silicic seal. While this architecture may not fully reflect our current understanding of transcrustal magmatic systems (e.g., Cashman et al., 2017), our observations of a relatively tabular intrusion, and the lack of any notable degassing suggest magma accumulation either below some barrier or into a pre-existing weakness. Combined with observations at, for instance, Laguna del Maule in Chile (e.g., Le Mével et al., 2021) which exhibits large and time varying deformation, we hypothesize that the observed deformation can similarly be explained by either an intrusion of mafic magma into a silicic reservoir or underplating of basalt below a silicic seal. The time delay between onset of the intrusion and seismicity detectable at about 25 km distance is likely due to relatively ductile material at depth through which the mafic magma rises without creating noticeable seismicity at that distance and the inflation drives the fracturing of the overlying rock column, not the movement of magma. This is supported by the proximity to the Queen-Charlotte Fairweather Transform Fault, separating the oceanic Pacific Plate from the North American plate, supporting higher heat flux.

While it is not uncommon for volcanoes to deform, the activity at Mt. Edgumbe is somewhat unique as reactivation of a dormant volcanic system, especially in large transform settings, is rarely observed. One recent similar case is perhaps the 2021 Icelandic Mt. Fagradalsfjall eruption on the Reykjanes Peninsula, an oblique rifting environment, which triggered strike slip earthquakes and released tectonic stresses accumulated over long time periods after 800 years with no eruption (Sigmundsson et al., 2021). In classic subduction settings, Mt. Peulik in Alaska inflated from 1996-1998 at rates very similar to those we observed here, not resulting in an eruption (Lu et al., 2002). Mével et al. (2015) finds commonalities in the deformation between Laguna del Maule, Yellowstone, Long Valley, and Three Sisters, suggesting that high rates of deformation over long timescales (more than 8 years) and varying displacement rates over time are not uncommon and do not necessarily result in an eruption.

6 Conclusions

A seismic swarm in 2022 near Mt. Edgumbe (L'ux Shaa), Southeast Alaska, inspired retrospective analysis of seismic and SAR data spanning the time period between 2018-2022, and 2014-2022, respectively. Aided by open, cloud-native data and tools, we generated InSAR time series and stable deformation models just days after the onset of

seismic unrest, with most of the time spent on different kinds of re-analysis to ensure reliability of our results. The InSAR time series analysis indicates no deformation until August of 2018 when rapid linear inflation at rates up to 8.7 cm/yr in the satellite LOS set on. The cumulative deformation over more than 3 years reaches as much as 27 cm in LOS centered about 2-3 km east of Mt. Edgecumbe and has a radius of about 17 km. We find the deformation to be consistent with a slightly westward dipping tabular body inflating between 5.3-7.6 km depth, striking north-northwest, and extending in length and width about 9 km and 8 km, respectively. With a cumulative opening of 0.65 m, we estimate about 52×10^6 m³ total magma intruded. The re-analysis of the seismicity shows that the regional network did not locate any earthquakes under Kruzof Island until January 2020 and seismicity detected on the single closest station does not markedly increase until July 2019. Thus, we suggest a mafic intrusion into or below ductile rhyolite that acts as a seal, preventing further rise and degassing. Any seismicity related to the intrusion may be too small to register at the distant seismograph, which records fracturing of the crust overlying the intrusion as strain built up through the inflation is released. This activity provides an excellent opportunity to understand the cyclicity of volcanic activity and the reawakening of dormant systems, especially in transform fault settings.

Acknowledgments

We thank Matt Haney, John Power, and Aaron Wech for helpful suggestions on the seismic analysis. This work was partially funded through a cooperative agreement between the USGS Volcano Hazard Center and UAF, which provides partial funding for the Alaska Volcano Observatory. In addition, RG acknowledges partial support from NSF-ICER 2019232; and MA, DT and DF acknowledge support from NSF-ICER 1855126. OpenSARLab was funded under NASA grants 80NSSC19K1109, 80NSSC20K0164, and 80NSSC18K0317. The ASF HyP3 development was funded by the NASA ASF DAAC. Copernicus Sentinel data from 2014-2022, retrieved from ASF DAAC, processed by ESA. Results generated using Copernicus Atmosphere Monitoring Service information.

Open Research

The SAR data analyzed are available through ESA and ASF DAAC. We use HyP3 (Hogenson et al., 2016; Johnston et al., 2022) and OSL (Hogenson et al., 2021; Meyer et al., 2021) workflows. The seismic data analyzed are available through the IRIS Data Management Center under network code 'AT' and station 'SIT'. We use the ObsPy seismological toolbox (Beyreuther et al., 2010) and REDPy (Hotovec-Ellis & Jeffries, 2016) for the seismic analysis. Earthquake locations are available as part of the USGS Comcat catalog (<https://earthquake.usgs.gov/data/comcat/>).

References

- Addison, J. A., Beget, J. E., Ager, T. A., & Finney, B. P. (2010). Marine tephrochronology of the Mt. Edgecumbe Volcanic Field, Southeast Alaska, USA. *Quaternary Research*, 73(2), 277–292. doi: 10.1016/j.yqres.2009.10.007
- Agram, P., & Jolivet, R. (2012). *Variable resolution subsampler for InSAR data*. Seismological Laboratory Caltech. Retrieved from https://github.com/ericlindsey/varres/{_}gmtsar/blob/master/var/{_}res/{_}doc.pdf
- Allen, R. V. (1978). Automatic earthquake recognition and timing from single traces. *Bulletin of the Seismological Society of America*, 68(5), 1521–1532. Retrieved from <http://www.bssaonline.org/content/68/5/1521.short>
- Aster, R. C., Borchers, B., & Thurber, C. H. (2019). Iterative Methods. *Parameter Estimation and Inverse Problems*, 151–179. doi: 10.1016/b978-0-12-804651-7.00011-0
- Berardino, P., Fornaro, G., Lanari, R., & Sansosti, E. (2002). A new algorithm for

- surface deformation monitoring based on small baseline differential SAR interferograms. *IEEE Transactions on Geoscience and Remote Sensing*, 40(11), 2375–2383. doi: 10.1109/TGRS.2002.803792
- Beyreuther, M., Barsch, R., Krischer, L., Megies, T., Behr, Y., & Wassermann, J. (2010, may). ObsPy: A Python Toolbox for Seismology. *Seismological Research Letters*, 81(3), 530–533. Retrieved from <https://pubs.geoscienceworld.org/srl/article/81/3/530-533/143693> doi: 10.1785/gssrl.81.3.530
- Borsa, A. A., Agnew, D. C., & Cayan, D. R. (2014, sep). Ongoing drought-induced uplift in the western United States. *Science*, 345(6204), 1587–1590. Retrieved from <http://www.ncbi.nlm.nih.gov/pubmed/25147281><http://www.sciencemag.org/cgi/doi/10.1126/science.1260279> doi: 10.1126/science.1260279
- Cashman, K. V., Sparks, R. S. J., & Blundy, J. D. (2017). Vertically extensive and unstable magmatic systems: A unified view of igneous processes. *Science*, 355(6331). doi: 10.1126/science.aag3055
- Chen, C. W., & Zebker, H. A. (2002). Phase unwrapping for large SAR interferograms: Statistical segmentation and generalized network models. *IEEE Transactions on Geoscience and Remote Sensing*, 40(8), 1709–1719. doi: 10.1109/TGRS.2002.802453
- Compton, K., Bennett, R. A., & Hreinsdóttir, S. (2015, feb). Climate-driven vertical acceleration of Icelandic crust measured by continuous GPS geodesy. *Geophysical Research Letters*, 42(3), 743–750. Retrieved from <http://doi.wiley.com/10.1002/2014GL062446> doi: 10.1002/2014GL062446
- Elliott, J., & Freymueller, J. T. (2020a). A Block Model of Present-Day Kinematics of Alaska and Western Canada. *Journal of Geophysical Research: Solid Earth*, 125(7), 1–30. doi: 10.1029/2019JB018378
- Elliott, J., & Freymueller, J. T. (2020b). Kinematics of the Fairweather-Queen Charlotte Transform System and Deformation of the Northeast Pacific plate. In *American geophysical union, fall meeting* (pp. T050–09). Retrieved from <https://ui.adsabs.harvard.edu/abs/2020AGUFMT050...09E>
- Elliott, J. L., Larsen, C. F., Freymueller, J. T., & Motyka, R. J. (2010, sep). Tectonic block motion and glacial isostatic adjustment in southeast Alaska and adjacent Canada constrained by GPS measurements. *Journal of Geophysical Research*, 115(B9), B09407. Retrieved from <http://doi.wiley.com/10.1029/2009JB007139> doi: 10.1029/2009JB007139
- ESA. (2022). *Copernicus Sentinel-1B anomaly (6th update)*. Retrieved 2022-05-04, from <https://sentinels.copernicus.eu/web/sentinel/-/copernicus-sentinel-1b-anomaly-6th-update/1.1>
- Fattahi, H., & Amelung, F. (2013). DEM error correction in InSAR time series. *IEEE Transactions on Geoscience and Remote Sensing*, 51(7), 4249–4259. doi: 10.1109/TGRS.2012.2227761
- Fialko, Y., Khazan, Y., & Simons, M. (2001, jul). Deformation due to a pressurized horizontal circular crack in an elastic half-space, with applications to volcano geodesy. *Geophysical Journal International*, 146(1), 181–190. Retrieved from <http://doi.wiley.com/10.1046/j.1365-246X.2001.00452.x> doi: 10.1046/j.1365-246X.2001.00452.x
- Grapenthin, R., Sigmundsson, F., Geirsson, H., Árnadóttir, T., & Pinel, V. (2006). Icelandic rhythmicity: Annual modulation of land elevation and plate spreading by snow load. *Geophysical Research Letters*, 33(24). doi: 10.1029/2006GL028081
- Haario, H., Saksman, E., & Tamminen, J. (2001). An adaptive Metropolis algorithm. *Bernoulli*, 7(2), 223–242. doi: 10.2307/3318737
- Heki, K. (2001). Seasonal Modulation of Interseismic Strain Buildup in Northeastern Japan Driven by Snow Loads. *Science*, 293, 89–92.

- Hersbach, H., Bell, B., Berrisford, P., Hirahara, S., Horányi, A., Muñoz-Sabater, J., ... Thépaut, J. N. (2020). The ERA5 global reanalysis. *Quarterly Journal of the Royal Meteorological Society*, 146(730), 1999–2049. doi: 10.1002/qj.3803
- Hogenson, K., Arko, S. A., Buechler, B., Hogenson, R., Herrmann, J., & Geiger, A. (2016). Hybrid Pluggable Processing Pipeline (HyP3): A cloud-based infrastructure for generic processing of SAR data. In *Agu fall meeting abstracts* (Vol. 2016, pp. IN21B—1740).
- Hogenson, K., Meyer, F. J., Logan, T. A., Lewandowski, A., Stern, T., Lundell, E., & Miller, R. R. (2021). The ASF OpenSARLab—A cloud-based (SAR) Remote Sensing Data Analysis Platform. In *Agu fall meeting 2021*.
- Hotovec-Ellis, A. J., & Jeffries, C. (2016). Near real-time detection, clustering, and analysis of repeating earthquakes: Application to Mount St. Helens and Redoubt volcanoes. In *Seismological society of america annual meeting*.
- Hotovec-Ellis, A. J., Shiro, B. R., Shelly, D. R., Anderson, K. R., Haney, M. M., Thelen, W. A., ... Johanson, I. A. (2022). Earthquake-Derived Seismic Velocity Changes During the 2018 Caldera Collapse of Kīlauea Volcano. *Journal of Geophysical Research: Solid Earth*, 127(2). doi: 10.1029/2021JB023324
- Hu, Y., & Freymueller, J. T. (2019). Geodetic Observations of Time-Variable Glacial Isostatic Adjustment in Southeast Alaska and Its Implications for Earth Rheology. *Journal of Geophysical Research: Solid Earth*, 124(9), 9870–9889. doi: 10.1029/2018JB017028
- Jellinek, A. M., Manga, M., & Saar, M. O. (2004). Did melting glaciers cause volcanic eruptions in eastern California? Probing the mechanics of dike formation. *J. Geophys. Res.*, 109, B09206. doi: 10.1029/2004JB002978
- Johnston, A., Rine, J., Kennedy, J. H., Herrmann, J., Jacquelynsmale, Cirrusasf, & Kristenson, H. (2022, may). *ASFHyP3/hyp3: HyP3 v2.16.0*. Zenodo. Retrieved from <https://doi.org/10.5281/zenodo.6518576> doi: 10.5281/zenodo.6518576
- Jull, M., & McKenzie, D. (1996). The effect of deglaciation on mantle melting beneath Iceland. *Journal of Geophysical Research*, 101, 21,815–821,828. doi: 10.1029/96JB01308
- Kitka, H. (n.d.). *The Legend of Shee Atika*.
- Larsen, C. F., Motyka, R. J., Freymueller, J. T., Echelmeyer, K. A., & Ivins, E. R. (2004, jul). Rapid uplift of southern Alaska caused by recent ice loss. *Geophysical Journal International*, 158(3), 1118–1133. Retrieved from <https://academic.oup.com/gji/article-lookup/doi/10.1111/j.1365-246X.2004.02356.x> doi: 10.1111/j.1365-246X.2004.02356.x
- Larsen, C. F., Motyka, R. J., Freymueller, J. T., Echelmeyer, K. A., & Ivins, E. R. (2005). Rapid viscoelastic uplift in southeast Alaska caused by post-Little Ice Age glacial retreat. *Earth and Planetary Science Letters*, 237(3-4), 548–560. doi: 10.1016/j.epsl.2005.06.032
- Le Mével, H., Córdova, L., Cardona, C., & Feigl, K. L. (2021). Unrest at the Laguna del Maule volcanic field 2005–2020: renewed acceleration of deformation. *Bulletin of Volcanology*, 83(6). doi: 10.1007/s00445-021-01457-0
- Lu, Z., Wicks, C., Dzurisin, D., Power, J. A., Moran, S. C., & Thatcher, W. (2002). Magmatic inflation at a dormant stratovolcano: 1996-1998 activity at Mount Peulik volcano, Alaska, revealed by satellite radar interferometry. *Journal of Geophysical Research: Solid Earth*, 107(B7), ETG 4–1–ETG 4–13. doi: 10.1029/2001jb000471
- MacLennan, J., Jull, M., Mckenzie, D., Slater, L., & Gro, K. (2002). The link between volcanism and deglaciation in Iceland. *Geochemistry Geophysics Geosystems*, 1–25. doi: 10.1029/2001GC000282
- Mével, H. L., Feigl, K. L., Córdova, L., DeMets, C., & Lundgren, P. (2015). Evolution of unrest at Laguna del Maule volcanic field (Chile) from InSAR and GPS measurements, 2003 to 2014. *Geophysical Research Letters*, 42(16), 6590–6598.

- doi: 10.1002/2015GL064665
- Meyer, F. J., Rosen, P. A., Flores, A., Anderson, E. R., & Cherrington, E. A. (2021). Making Sar Accessible: Education & Training in Preparation for Nisar. In *2021 IEEE International Geoscience and Remote Sensing Symposium IGARSS* (pp. 6–9).
- Mogi, K. (1958). Relations between eruptions of various volcanoes and the deformations of the ground surface around them. *Bull. Earthquake Res. Inst. Univ. Tokyo*, 36, 99–134.
- Okada, Y. (1992). Internal deformation due to shear and tensile faults in a half-space. *Bull. Seis. Soc. Am.*, 82(2), 1018–1040.
- Pagli, C., & Sigmundsson, F. (2008, may). Will present day glacier retreat increase volcanic activity? Stress induced by recent glacier retreat and its effect on magmatism at the Vatnajökull ice cap, Iceland. *Geophysical Research Letters*, 35(9), L09304. Retrieved from <http://doi.wiley.com/10.1029/2008GL033510> doi: 10.1029/2008GL033510
- Patil, A., Huard, D., & Fonnesbeck, C. J. (2010, jul). PyMC: Bayesian Stochastic Modelling in Python. *Journal of statistical software*, 35(4), 1–81. Retrieved from <http://www.ncbi.nlm.nih.gov/pubmed/21603108><http://www.pubmedcentral.nih.gov/articlerender.fcgi?artid=PMC3097064>
- Praetorius, S., Mix, A., Jensen, B., Froese, D., Milne, G., Wolhowe, M., ... Prahl, F. (2016). Interaction between climate, volcanism, and isostatic rebound in Southeast Alaska during the last deglaciation. *Earth and Planetary Science Letters*, 452, 79–89. Retrieved from <http://dx.doi.org/10.1016/j.epsl.2016.07.033> doi: 10.1016/j.epsl.2016.07.033
- Press, W. H., Teukolsky, S. A., Vetterling, W. T., & Flannery, B. P. (2007). *Numerical Recipes: The Art of Scientific Computing* (3rd ed.). Cambridge University Press.
- Riehle, J. R., Champion, D. E., Brew, D. A., & Lanphere, M. A. (1992). Pyroclastic deposits of the Mount Edgecumbe volcanic field, southeast Alaska: eruptions of a stratified magma chamber. *Journal of Volcanology and Geothermal Research*, 53(1-4), 117–143. doi: 10.1016/0377-0273(92)90078-R
- Schell, M. M., & Ruff, L. J. (1989). Rupture of a seismic gap in southeastern Alaska: the 1972 Sitka earthquake (Ms 7.6). *Physics of the Earth and Planetary Interiors*, 54(3-4), 241–257. doi: 10.1016/0031-9201(89)90246-X
- Sigmundsson, F., Parks, M., Hooper, A. J., Geirsson, H., Vogfjörð, K. S., Drouin, V., ... Others (2021). Un-stressing of crust prior to eruptions: Precursors to the 2021 eruption at Geldingadalir, Mt. Fagradalsfjall, in the Reykjanes Peninsula Oblique Rift, Iceland. In *Agu fall meeting 2021*.
- Torres, R., Snoeij, P., Geudtner, D., Bibby, D., Davidson, M., Attema, E., ... Rostan, F. (2012). GMES Sentinel-1 mission. *Remote Sensing of Environment*, 120, 9–24. Retrieved from <http://dx.doi.org/10.1016/j.rse.2011.05.028> doi: 10.1016/j.rse.2011.05.028
- Wegnüller, U., Werner, C., Strozzi, T., Wiesmann, A., Frey, O., & Santoro, M. (2016). Sentinel-1 Support in the GAMMA Software. *Procedia Computer Science*, 100, 1305–1312. Retrieved from <http://dx.doi.org/10.1016/j.procs.2016.09.246> doi: 10.1016/j.procs.2016.09.246
- Wellik, J. J., Prejean, S. G., & Syahbana, D. K. (2021). Repeating Earthquakes During Multiple Phases of Unrest and Eruption at Mount Agung, Bali, Indonesia, 2017. *Frontiers in Earth Science*, 9(May), 1–11. doi: 10.3389/feart.2021.653164
- Woolsey, R. (2021). *Private dock projected to double Sitka cruise passengers in 2022*. Retrieved from <https://www.ktoo.org/2021/09/08/private-dock-projected-to-double-sitka-cruise-passengers-in-2022/>
- Yang, X. M., Davis, P. M., & Dieterich, J. H. (1988). Deformation from Inflation of a Dipping Finite Prolate Spheroid in an Elastic Half-Space as a Model for

511 Volcanic Stressing. *Journal of Geophysical Research*, 93, 4257–4549.
512 Yunjun, Z., Fattahi, H., & Amelung, F. (2019). Small baseline InSAR time se-
513 ries analysis: Unwrapping error correction and noise reduction. *Computers and*
514 *Geosciences*, 133(May), 104331. Retrieved from [https://doi.org/10.1016/j](https://doi.org/10.1016/j.cageo.2019.104331)
515 [.cageo.2019.104331](https://doi.org/10.1016/j.cageo.2019.104331) doi: 10.1016/j.cageo.2019.104331